Machine learning-based emulator for the physics-based simulation of auroral current system

Ryuho Kataoka[1,2], Aoi Nakamizo[3], Shinya Nakano[4,5,2], Shigeru Fujita[4,5]

[1] National Institute of Polar Research, Tachikawa, 190-8518, Japan

[2] SOKENDAI, Tachikawa, 190-8518, Japan

[3] National Institute of Information and Communications Technology, Koganei, 184-8795, Japan

[4] The Institute of Statistical Mathematics, Tachikawa, 190-8562, Japan

[5] Center for Data Assimilation Research and Applications, Joint Support Center for Data Science Research, Tachikawa, 190-8562, Japan

Corresponding author: Ryuho Kataoka (kataoka.ryuho@nipr.ac.jp)

Key Points:

- We developed machine learning-based emulator for surrogating the ionospheric outputs of a global MHD simulation called REPPU.
- The new emulator model SMRAI2 runs million times faster than the original physics-based simulation.
- The new emulator model SMRAI2 can be utilized for the real-time space weather forecast of auroral current system.

Abstract

Using a machine learning technique called echo state network (ESN), we have developed an emulator to model the physics-based global magnetohydrodynamic (MHD) simulation results of REPPU (REProduce Plasma Universe) code. The inputs are the solar wind time series with date and time, and the outputs are the time series of the ionospheric auroral current system in the form of two-dimensional (2D) patterns of field-aligned current, potential, and conductivity. We mediated a principal component analysis for a dimensionality reduction of the 2D map time series. In this study, we report the latest upgraded Surrogate Model for REPPU Auroral Ionosphere version 2 (SMRAI2) with significantly improved resolutions in time and space (5 min in time, ~1 degrees in latitude, and 4.5 degrees in longitude), where the dipole tilt angle is also newly added as one of the input parameters to reproduce the seasonal dependence. The fundamental dependencies of the steady-state potential and field-aligned current patterns on the interplanetary magnetic field (IMF) directions are consistent with those obtained from empirical models. Further, we show that the ESN-based emulator can output the AE index so that we can evaluate the performance of the dynamically changing results, comparing with the observed AE index. Since the ESN-based emulator runs a million times faster than the REPPU simulation, it is promising that we can utilize the emulator for the real-time space weather forecast of the auroral current system as well as to obtain large-number ensembles to achieve future data assimilation-based forecast.

Plain Language Summary

Physics-based auroral simulations, such as Japanese REPPU code, are not practically fast enough for the purpose of real-time space weather forecast, even using the designated super computers. Here we developed a million-times-faster “emulator” to surrogate the outputs of the physics-based simulation, using the machine-learning technique called Echo State Network. The newly developed emulator, the surrogate model for REPPU auroral Ionosphere version 2 (SMRAI2) enables us to realize the real-time forecast of the auroral current system.

1 Introduction

Forecasting the auroral current system in the polar regions has been one of the core parts of the operational space weather forecast because the auroral current system is the origin of the enhanced satellite drag via the Joule heat in the thermosphere. In recent years, such an importance has been especially growing, and the spacecraft operations are getting more sensitive along the heavy utilization of the low-earth orbit. For example, it was remarkable that as many as 38 commercial satellites lost at the same time during moderate storms in February 2022 (e.g., Kataoka et al., 2022). The auroral current system, including auroral electrojet activities as known by the AE index, has been of fundamental importance for other various space weather aspects, including geomagnetically induced currents (GIC) flowing along the ground-based infrastructures (e.g., Kataoka and Ngwira, 2016), and satellite charging and communications malfunctions.

On the other hand, there is a long history of conducting physics-based simulations to understand the variable polar ionosphere (Lyon et al., 1980; Ogino, 1986). Because of the nonlinear nature of the spatially complex evolution of auroral ovals and the magnetospheric plasma flows as driven by the time-varying solar wind conditions, a global magnetohydrodynamic (MHD) simulation with the input of the solar wind parameters is

necessary to reproduce the resultant auroral current system, as depicted by the ionospheric conductivities, potential, and field-aligned currents. Among many sophisticated MHD simulations, REPPU (REProduce Plasma Universe) has been known as one of the best models for resolving various space weather phenomena including auroral substorms (Ebihara et al., 2015a; 2015b; Tanaka et al., 2017; 2018; 2022b). However, the major difficulty of REPPU and other simulation codes for the operational space weather forecast is that it is time-consuming to solve the MHD equations, even using the designated cluster computers.

This study shows that the latest development in machine learning techniques can help solve this time-consuming issue. The very initial approach of such an emulator version 1.0 was proposed by Kataoka et al. (2023), using the time-dependent machine learning model called echo state network (ESN). In this study, we conducted a major upgrade of the ESN-based emulator by training the emulator model using an order of magnitude larger amount of the REPPU simulation outputs from that of ver1.0, as conducted by the long-term simulation runs (Nakamizo and Kubota, 2021) under the space weather forecast operations at National Institute of Information and Communications Technology (NICT).

In Section 2 we describe the REPPU simulation code and explain the technical details of the machine-learning model, especially focusing on how to emulate the REPPU simulation's ionospheric outputs. In Section 3, we show the primary results of the new emulator model. In Section 4, we discuss the performance and the limitation. Concluding remarks are briefly summarized in Section 5.

2 Methods

2.1 Magnetohydrodynamic simulation code: REPPU

REPPU is an MHD simulation code developed for studying the global magnetosphere-ionosphere coupling (Tanaka, 1995; Tanaka, 2015). The REPPU code is characterized by an excellent ionospheric reproduction of fundamental auroral phenomena such as substorms (Ebihara and Tanaka, 2015a; 2015b), sun-aligned arcs (Tanaka et al., 2017), and the theta aurora (Tanaka et al., 2018). In this study, we used an improved REPPU simulation code (Nakamizo and Kubota, 2021), including the effects of a tilted dipole axis and seasonal changes of solar zenith angles. The total number of grid cells in the magnetosphere is 30722 (horizontal) × 240 (vertical), where the unstructured grid system (Moriguchi et al., 2008; Nakamizo et al., 2009) is employed. The number of grid cells in the ionosphere is 30722. In this study, for the training and testing data, we took only the northern polar ionosphere, i.e. 30×80 pixels in latitude and longitude, after applying the 2×4 binning in latitude and longitude. The ionospheric outputs of the field-aligned current J//, conductivities Σxx (north-south), Σxy (off-diagonal), Σyy (east-west), and ionospheric potential Φ are saved every min, where the current continuity equation at the two-dimensional height-integrated ionosphere (x: north-south, y: east-west) is satisfied as:

$$J_{\parallel} = \nabla \cdot \mathbf{J}_{\perp} = \nabla \cdot \left(\tilde{\Sigma} \cdot \mathbf{E} \right), \tag{1}$$

$$\tilde{\Sigma} = \begin{pmatrix} \Sigma_{xx} & \Sigma_{xy} \\ -\Sigma_{xy} & \Sigma_{yy} \end{pmatrix}, \tag{2}$$

$$\mathbf{E} = \left(-\frac{\partial \Phi}{\partial x}, -\frac{\partial \Phi}{\partial y} \right). \quad (3)$$

The interplanetary magnetic field (IMF) Bx, By, and Bz are defined in the GSM (Geocentric Solar Magnetospheric) coordinate system. The real-time solar wind data (IMF Bx, By, Bz, solar wind speed V, proton density Np, and temperature Tp) at 1 min resolution was linearly interpolated if there was a data gap and used as the input time series to run the REPPU simulations. The real-time solar wind data can differ from the finally calibrated solar wind data, such as OMNI dataset. Nevertheless, it is essentially little problem for the machine-learning model to learn the REPPU simulation results for variable input patterns.

NICT team has been operating the real-time simulation with the improved REPPU code for the space weather forecast (Nakamizo and Kubota, 2021). The REPPU simulation has been running on the High-Performance Computing System at NICT since August, 2020. The simulation-run basically works automatically. Still, it is sometimes manually stopped and restarted due to some failures of the computing system, such as the system maintenances and failures of the simulation. The saved results are, therefore, not necessarily continuous.

In this study, we selected major interplanetary shock events and other large-amplitude events since 2021, including both predominantly southward and predominantly northward IMF conditions to include both storm-time and non-storm-time, respectively, as shown in **Table 1**. We also selected the long-term non-stop runs from December 2020 to January 2021 to compensate for the winter-time training data. Another long-term results from June to July 2021 is also prepared as the testing time interval.

2.2 Machine-learning model: Echo state network

The basic flow of the development of Surrogate Model for REPPU Auroral Ionosphere version 2 (SMRAI2) and the relationship of REPPU simulation and ESN model is graphically summarized in **Figure 1.** Firstly, we adopted the dimensionality reduction for the ionospheric outputs as obtained from REPPU simulations, by applying the principal component analysis (PCA) using the Python 3 scikit-learn/pca. Very similar method was used by Licata and Mehta (2023) for different purpose (thermosphere model emulator). The time series of each parameter z = {Σxy, Φ, or J//}, at certain (latitude, longitude) position of the grid indices (i ,j), can be represented by the time averaged spatial pattern z_0 and the linear combination of time-dependent PCA variables α and PCA component patterns U as follows:

$$z(i, j, t) = z_0(i, j) + z_1(i, j, t), \quad (4)$$

$$z_1(i, j, t) = \sum_{r=1}^{N_r} \alpha_r(t) U_r(i, j). \quad (5)$$

In this study, the numbers of PCA components Nr are selected to be 10 for Σxy and Φ, and 20 for J// to reconstruct >90% variance of the original features.

To those time-dependent PCA variables α, we employed essentially the same Echo State Network model (Jaeger, 2001; Jaeger and Haas, 2004; Tanaka et al., 2019) as Kataoka et al.

(2023) documented. In this study, we used the ESN module of Python 3 as developed by Tanaka et al. (2022a) (See https://github.com/GTANAKA-LAB/DTS-ESN/).

The ESN model used in this study is described by the reservoir state vector **x** and the model output vector **y** at $t = n + 1$ steps as follows:

$$\mathbf{x}(n+1) = \tanh\left\{W^{in}\mathbf{u}(n+1) + W\mathbf{x}(n)\right\}, \tag{6}$$

$$\mathbf{y}(n+1) = W^{out}\mathbf{x}(n+1). \tag{7}$$

Here, the weight matrices W^{in} and W are multiplied by the input vector **u** (the solar wind time series) and the reservoir state vector **x**, respectively. We create the random and sparse node connections of W^{in} and W, where only 10% of the matrix elements are random values between -1.0 and 1.0, and the remaining 90% are zero. The weight matrices W^{in} and W are fixed, while only Wout is trained by the ridge regression with the regularization parameter $\beta = 10^{-3}$ to minimize the objective function F,

$$F = \sum_{n=1}^{N} \left\|\mathbf{y}(n) - \mathbf{d}(n)\right\| + \frac{\beta}{2}\left\|W^{out}\right\|^2, \tag{8}$$

where **d** is a desired data vector consisting of the time series of the PCA variables of J//, Σxy, and Φ.

As the input vectors u, the solar wind speed and density are normalized as $\log_{10}$ V - 2.5, and $\log_{10}$ Np - 1.0, respectively, before training the ESN model because both the solar wind speed and density follow log-normal distributions (Burlaga and Lazarus, 2000). The IMF By and Bz components are also used as the input parameters. Further, the dipole tilt angle is newly introduced as the input to adopt the model for all seasons. The dipole tilt angle is calculated from the date and time by Python 3 pyspedas/geopack.

The emulator was trained by 107-day worth of outputs (30816 time steps) of REPPU simulation results. The testing data is 52 days, including both quiet and active months. The selection of training data and testing data was summarized in **Table 1**. The basic specifications of ESN-based emulators ver1.0 and ver2.0 are summarized in **Table 2**.

We optimized the number of the nodes (elements of x) to be 400, 250, and 300 for J//, Φ, and Σxy, respectively, and the spectral radius (maximum eigenvalue of W) to be 0.99 for all J//, Φ, and Σxy, by finding the minimum values of the normalized root-mean-square errors (NRMSE) using the testing data for the first PCA variables. From these results, the constructed emulator model has NRMSE of ~0.7, ~0.5, and ~0.8 to reconstruct the first PCA variables of J//, Φ, and Σxy, respectively.

In this study, we independently constructed the emulators for J//, Σxy, and Φ maps. However, the current continuity Eq. (1) relates these parameters, and any inconsistencies among these parameters can therefore give hints to evaluate the deviations in the emulation results for future applications.

It takes less than 10 s for the emulator to calculate a 1-day variation of auroral current system using a single node. In contrast, it takes ~5 days for the REPPU simulation to calculate the same 1-day variation using the 30-node cluster computer. Therefore, the computational cost of the SMRAI2 is approximately a million times more efficient than the original physics-based REPPU simulation.

3 Results

One of the major upgrades of SMRAI2 from the emulator ver1.0 (Kataoka et al., 2023) is the dipole tilt angle dependence by learning the simulation outputs from different seasons. From the steady state conditions for different tilt angles, **Figure 2** shows that the trained model learned the tilt angle dependence of the Hall conductivity Σxy. Notably, the dayside conductivity is high in the summer season, while the nightside conductivity is low in the summer. The obtained tendency of the nightside conductivity is consistent with the results of Newell et al. (2010).

Figure 3 shows the IMF clock angle dependence of the Region-1 and Region-2 field-aligned current system (Iijima and Potemra, 1978). The IMF clock angle is defined as the angle made in the By-Bz space, i.e., atan(By/Bz). We picked up the steady-state conditions of SMRAI2 results for each input parameter to make this figure. The overall IMF clock angle dependence and the amplitude of J// are reasonable, and consistent with empirical models such as Weimer (2001a). Further, we can see the IMF By dependent cusp current system in the higher latitude region than the Region 1 currents (Fujii and Iijima, 1980), especially during the northward IMF conditions.

Figure 4 shows the IMF clock angle dependence of the ionospheric potential, almost the same with the results from the emulator ver1.0 (Kataoka et al., 2023), consistent with empirical models such as Weimer-2K model (Weimer, 2001b) as shown in **Figure 5**. Comparing Figures 4 and 5, the IMF By dependent appearances of the crescent- and round-shaped cells are clearly captured. However, the amplitude of cross-polar cap potential is only ~60% compared to the empirical models. Such an underestimating tendency is naturally expected, as we adopted the coarse-graining of ionospheric potential such as the binning and PCA analysis. We will come back to this point later.

4 Discussions

One way to examine the performance of the SMRAI2 using the open data is to calculate the AE index (https://wdc.kugi.kyoto-u.ac.jp/aedir/index.html) from the emulator and compare it with the observed values. In this study, we calculate the AU/AL indices (AE = AU - AL) from the emulator results with the electric field as estimated by the spatial derivatives of Φ map using the central difference,

$$\left(\frac{\partial\Phi}{\partial x},\frac{\partial\Phi}{\partial y}\right)=\left(\frac{\Phi_{i+1}-\Phi_{i-1}}{2\Delta x},\frac{\Phi_{j+1}-\Phi_{j-1}}{2\Delta y}\right), \tag{9}$$

where i and j are the indices of latitude and longitude, respectively, and the Δx (north-south) and Δy (east-west) are calculated from the colatitude θ, longitude φ, and the Earth radius R_E as

$$\left(\Delta x,\ \Delta y\right)=\left(\frac{\Delta\theta}{360}2\pi R_E,\ \frac{\Delta\varphi}{360}2\pi R_E\sin\theta\right). \tag{10}$$

The ionospheric Hall current vectors are then calculated as

$$\mathbf{J}_{Hall}=\left(\Sigma_{xy}E_y,-\Sigma_{xy}E_x\right)=\left(-\Sigma_{xy}\frac{\partial\Phi}{\partial y},\Sigma_{xy}\frac{\partial\Phi}{\partial x}\right). \tag{11}$$

We then applied the so-called equivalent current theorem (Maeda, 1955; Fukushima, 1969; 1976) where the east-west component of the Hall current in the unit of A km^{-1} is nearly equal to the north-south component of the magnetic field at the ground in the unit of nT to calculate the AU/AL indices from the envelopes of the emulator outputs. The magnetic latitude range for the AU/AL calculation is selected from 60^o to 70^o.

The resultant AU and AL indices are shown in **Figure 6** for the one-month time interval, using the 5-min OMNI solar wind data. The data gaps of the OMNI 5-min data were filled by the forward interpolation using the Python 3 pandas/fillna/ffill method. **Figure 7** shows the 2D histogram for the 15-year results, indicating that the ESN-based emulator tends to underestimate the AE index. The cross-correlation coefficients between observed and emulated indices for the 15-year data are 0.592, 0.596, 0.666 for AU, AL, and AE indices, respectively.

There are multiple causes for this underestimation of the AE index. First, it is natural to expect that the coarse-graining of ionospheric potential, such as the binning and PCA analysis must give smaller values than the original simulation results, as we pointed out at the end of Section 3. Also, the finite difference of **Equation 9** can further give the underestimation of the electric field, which was used to calculate the Hall current and the AE index. Therefore, having such a smaller AE index estimation by the ESN-based emulator is not surprising. Instead, we can use the SMRAI2 results as the fair values for the AE index prediction with the possible errors, as shown in **Figure 7**.

Since the AE index roughly represents the macroscopic energy release in the polar ionosphere, we can diagnose some hidden characteristics of the new SMRAI2 via inputting the synthetic solar wind data. We prepared the synthetic solar wind data to pick up the peak values of the predicted AE index during the 80 min time interval after the southward IMF turnings from the steady state of the northward IMF Bz = 1.0 nT, changing the IMF amplitude, solar wind speed, and density. Ebihara and Tanaka (2019) showed, using the REPPU simulations, that the positive density dependence of the auroral electrojet intensity is clear during weakly southward IMF, while it is not likely the same during strongly southward IMF. Similarly complex tendency for the density appeared in the results from the emulator ver2.0, as shown in the right panel of **Figure 8**. In contrast to the density, the dependence of the AE peak intensity on the solar wind speed is relatively simple, as linearly correlating with the product of southward IMF Bz and solar wind speed V, which was seen in both Ebihara and Tanaka (2019) as well as in the left panel of **Figure 8**.

Although it is improved from ver1.0 (Kataoka et al., 2023), the temporal resolution of 5 min still gives the major limitation of the SMRAI2. For example, we cannot discuss the highly dynamic phenomena such as the substorm onset and sudden commencement, in which all

ionospheric parameters drastically evolve in a short time scale of less than 5 min. Those rapid variation can cause large-amplitude GIC events, which is one of the important targets of the operational space weather forecast. One of the future works, therefore, include improving of the temporal resolution to 1 min since the ESN method can be applied to diverse temporal scales (Tanaka et al., 2022a). Caveat should also be made here that it may not so simply work to solve the substorm-onset-related problems by improving the temporal resolution because there is an essential difficulty in reproducing the variation just before and after the substorm onsets, as coming from the probabilistic nature of the substorm onsets (Nakano and Kataoka, 2022; Nakano et al., 2023).

Therefore, another natural next step would be the data assimilation of the SMRAI2 emulator to correct the exact timing of the substorm onset and the amplitude via the observation data. The million-times faster SMRAI2 emulator has a significant advantage in this direction, compared to the physics-based simulation, because it is essential to increase the ensemble number necessary for data assimilation. For realizing the data assimilation-based forecast, it would be reasonable to use any partial data or point data which is available for real-time use via applying the cutting-edge data assimilation techniques (Nakano et al., 2020).

5 Conclusions

We showed that SMRAI2 emulator model is ready-to-use for the real-time space weather forecast of the auroral current system for both the northern and southern hemispheres. We developed the latest upgraded version 2.0 of the ESN-based emulator for the REPPU simulation's ionospheric outputs of the field-aligned current, potential, and conductivity, which runs a million times faster than the REPPU code. The resolutions of the latest ESN-based emulator ver2.0 are significantly improved in time, latitude, and longitude, compared to the ver1.0, and the dipole tilt angle is also newly introduced as one of the input parameters, in addition to IMF By, Bz, V, and Np, thanks to an order of magnitude larger training dataset. We confirmed that the IMF clock-angle dependence of the auroral current system is consistent with that obtained from empirical models. New functions of the ESN-based emulator ver2.0 includes automatic OMNI solar wind data input and the AE index output by indicating the date only.

Acknowledgments

We acknowledge the use of NASA's high-resolution OMNI data and the Kyoto University's AE index data. The REPPU simulation was performed with High-Performance Computing System at NICT. The real-time solar wind data were provided by National Oceanic and Atmospheric Administration's Space Weather Prediction Center (NOAA/SWPC). This research was supported by "Challenging Exploratory Research Projects for the Future" grant from the Research Organization of Information and Systems (ROIS). In addition, this study is part of the Science Program of Japanese Antarctic Research Expedition (JARE) Prioritized Research Project AJ1007 (Space environmental changes and atmospheric response explored from the polar cap), supported by NIPR under MEXT.

Open Research

The OMNI solar wind data with the AE/AU/AL indices are publicly available at https://omniweb.gsfc.nasa.gov/ow_min.html. The Python 3 codes and the training/testing datasets for the ESN-based emulator model, SMRAI2, used in this study are open to the public at https://github.com/ryuhokataoka/REPPU-ESN2 (v2.0.0 was released at doi.org/10.5281/zenodo.7955440).

References

Burlaga, L. F., & Lazarus, A. J. (2000) Lognormal distributions and spectra of solar wind plasma fluctuations: Wind 1995-1998. Journal of Geophysical Research, 105(A2), 2357-2364. https://doi.org/10.1029/1999JA900442

Ebihara, Y., and T. Tanaka (2015a) Substorm simulation: Formation of westward traveling surge. Journal of Geophysical Research: Space Physics, 120(12), 10466-10484. https://doi.org/10.1002/2015JA021697

Ebihara, Y., and T. Tanaka (2015b) Substorm simulation: Insight into the mechanisms of initial brightening. Journal of Geophysical Research: Space Physics, 120(9), 7270?7288. https://doi.org/10.1002/2015JA021516

Ebihara, Y., Tanaka, T., & Kamiyoshikawa, N. (2019) New diagnosis for energy flow from solar wind to ionosphere during substorm: Global MHD simulation. Journal of Geophysical Research: Space Physics, 124, 360-378. https://doi.org/10.1029/2018JA026177

Fukushima, N. (1969) Equivalence in ground geomagnetic effect of Chapman-Vestine's and Birkeland-Alfven's current systems for polar magnetic storms. Rep. Ionos. Space Res. Jpn., 32, 219-227

Fukushima, N. (1976) Generalized theorem for no ground magnetic effect of vertical currents connected with Pedersen currents in the uniform-conductivity ionosphere. Rep. Ionos. Space Res. Jpn., 30, 35-40.

Iijima, T., and T. A. Potemra (1978) Large-scale characteristics of field-aligned currents associated with substorms, J. Geophys. Res., 83(A2), 599-615, doi:10.1029/JA083iA02p00599

Jaeger, H. (2001) The “echo state” approach to analysing and training recurrent neural networks GMD Report 148. German National Research Institute for Computer Science

Jaeger, H. and H. Haas (2004) Harnessing nonlinearity: Predicting chaotic systems and saving energy in wireless communication, Science, 304, 78-80, https://doi.org/10.1126/science.1091277

Kataoka, R., D. Shiota, H. Fujiwara, H. Jin, C. Tao, H. Shinagawa, and Y. Miyoshi (2022), Unexpected space weather causing the reentry of 38 Starlink satellites in February 2022, J. Space Weather and Space Climate, 41, 10, https://doi.org/10.1051/swsc/2022034.

Kataoka, R., S. Nakano, and S. Fujita (2023) Machine learning emulator for physics-based prediction of ionospheric potential response to solar wind variations, Earth, Planets and Space, 75, 139, doi:10.1186/s40623-023-01896-3.

Licata, R. J., and P. M. Mehta (2023) Reduced order probabilistic emulation for physics-based thermosphere models, Space Weather, 21, e2022SW003345, doi:10.1029/2022SW003345

Lyon, J., Brecht, S.H., Fedder, J.A. and Palmadesso, P. (1980) The effects on the Earth's magnetotail from shocks in the solar wind. Geophys. Res. Lett., 7: 721-724. https://doi.org/10.1029/GL007i009p00721

Maeda, H. (1955) Horizontal wind systems in the ionospheric E region deduced from the dynamo theory of the geomagnetic Sq variation, Part I. Non-rotating Earth, 7, 4, 121-132

Moriguchi, T., A. Nakamizo, T. Tanaka, T. Obara, and H. Shimazu (2008) Current systems in the Jovian magnetosphere, J. Geophys. Res., 113, A05204, doi:10.1029/2007JA012751

Nakamizo, A., T. Tanaka, Y. Kubo, S. Kamei, H. Shimazu, and H. Shinagawa (2009) Development of the 3-D MHD model of the solar corona-solar wind combining system, J. Geophys. Res., 114, A07109, doi:10.1029/2008JA013844

Nakamizo A., and Y. Kubota (2021) Research and Development of Global Magnetosphere MHD Simulation, NICT Research Report, Vol. 67, No. 1 (in Japanese with English abstract), https://www.nict.go.jp/data/research-report/index.html

Newell, P. T., Sotirelis, T., and Wing, S. (2010) Seasonal variations in diffuse, monoenergetic, and broadband aurora, J. Geophys. Res., 115, A03216, doi:10.1029/2009JA014805

Nakano, S., T. Hori, K. Seki, et al. (2020) A framework for estimating spherical vector fields using localized basis functions and its application to SuperDARN data processing. Earth Planets Space 72, 46. https://doi.org/10.1186/s40623-020-01168-4

Nakano, S. and R. Kataoka (2022) Echo state network model for analyzing solar-wind effects on the AU and AL indices, Ann. Geophys., 40, 11-22, https://doi.org/10.5194/angeo-40-11-2022

Nakano, S., R. Kataoka, M. Nose, and J. W. Gjerloev (2023) Probabilistic modelling of substorm occurrences with an echo state network, Ann. Geophys. Discuss. [preprint], https://doi.org/10.5194/angeo-2023-9, in review

Ogino, T.(1986) A three-dimensional MHD simulation of the interaction of the solar wind with the Earth's magnetosphere: The generation of field-aligned currents, J. Geophys. Res., 91(A6), 6791-6806, doi:10.1029/JA091iA06p06791

Tanaka, G., Yamane, T., Heroux, J. B., Nakane, R., Kanazawa, N., Takeda, S., et al. (2019) Recent advances in physical reservoir computing: A review. Neural Networks, 115, 100-123. https://doi.org/10.1016/j.neunet.2019.03.005

Tanaka, G., T. Matsumori, H. Yoshida, and K. Aihara (2022a) Reservoir computing with diverse timescales for prediction of multiscale dynamics, Phys. Rev. Research 4, L032014, doi:10.1103/PhysRevResearch.4.L032014

Tanaka, T. (1995) Generation mechanisms for magnetosphere-ionosphere current systems deduced from a three-dimensional MHD simulation of the solar wind-magnetosphere-ionosphere coupling processes. Journal of Geophysical Research, 100(A7), 12057-12074. https://doi.org/10.1029/95JA00419

Tanaka, T. (2015) Substorm Auroral Dynamics Reproduced by Advanced Global Magnetosphere-Ionosphere (M-I) Coupling Simulation. In Auroral Dynamics and Space Weather (eds Y. Zhang and L.J. Paxton). https://doi.org/10.1002/9781118978719.ch13

Tanaka, T., Obara, T., Watanabe, M., Fujita, S., Ebihara, Y., & Kataoka, R. (2017) Formation of the Sun-aligned arc region and the void (polar slot) under the null-separator structure. Journal of Geophysical Research: Space Physics, 122(4), 4102-4116. https://doi.org/10.1002/2016JA023584

Tanaka, T., Obara, T., Watanabe, M., Fujita, S., Ebihara, Y., Kataoka, R., & Den, M. (2018) Cooperatives roles of dynamics and topology in generating the magnetosphere-ionosphere disturbances: Case of the theta aurora. Journal of Geophysical Research: Space Physics, 123(12), 9991-10008. https://doi.org/10.1029/2018JA025514

Tanaka, T., Watanabe, M., Ebihara, Y., Fujita, S., Nishitani, N., & Kataoka, R. (2022b) Unified theory of the arc auroras: Formation mechanism of the arc auroras conforming general principles of convection and FAC generation. Journal of Geophysical Research: Space Physics, 127, e2022JA030403

Weimer, D. R. (1995) Models of high-latitude electric potentials derived with a least error fit of spherical harmonic coefficients, J. Geophys. Res., 100(A10), 19595-19607, doi:10.1029/95JA01755

Weimer, D. R. (2001a) Maps of ionospheric field-aligned currents as a function of the interplanetary magnetic field derived from Dynamics Explorer 2 data, J. Geophys. Res., 106(A7), 12889-12902, doi:10.1029/2000JA000295

Weimer, D. R. (2001b) An improved model of ionospheric electric potentials including substorm perturbations and applications to the Geospace environment modeling November 24, 1996, event, J. Geophys. Res., 106, 407-416, https://doi.org/10.1029/2000JA000604, 2001.

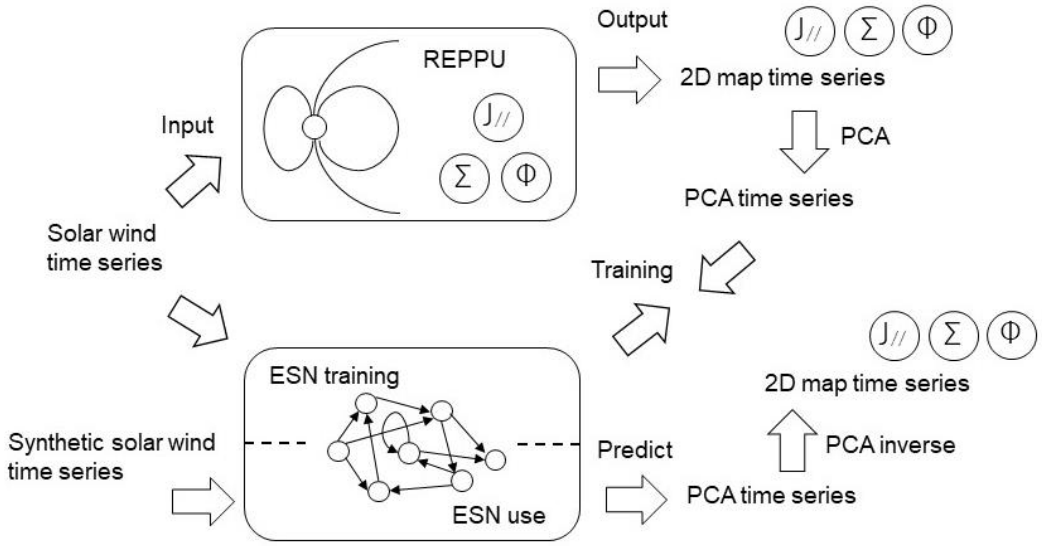

407

408 **Figure 1**. Block diagram of SMRAI2 development to graphically summarize the relationship
409 among the REPPU, PCA, and ESN.

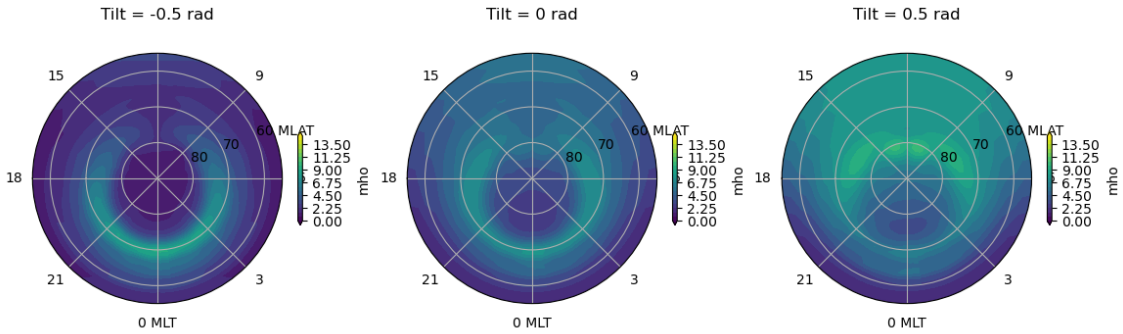

410

411 **Figure 2**. The tilt angle dependence of Σxy. Steady-state conditions of SMRAI2 are shown,
412 fixing the solar wind parameters By = 0.0 nT, Bz = 5.0 nT, Np = 5/cc, and Vsw = 400 km/s.

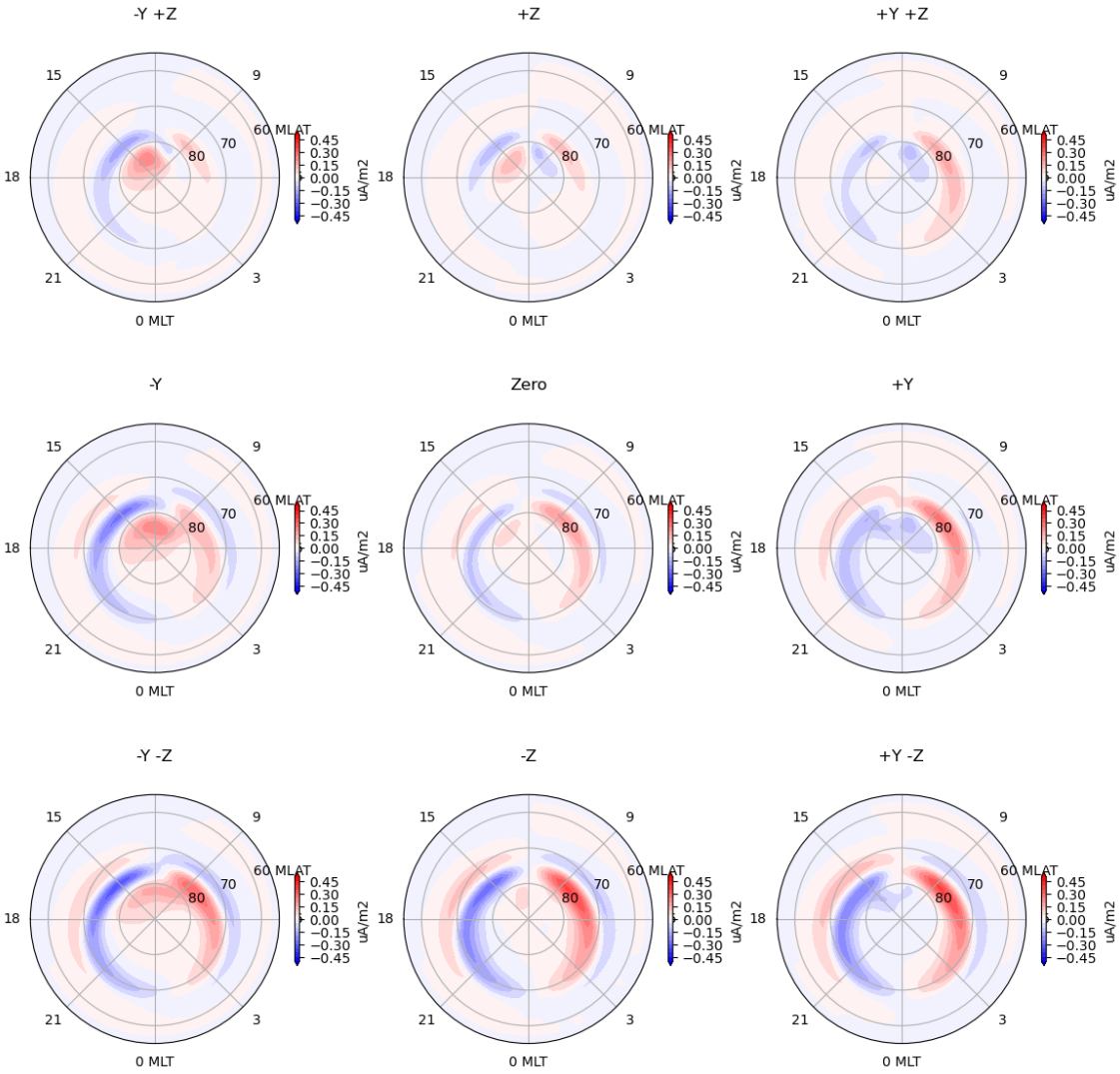

Figure 3. The IMF clock angle dependence of field-aligned current in the northern hemisphere. Steady-state conditions from the SMRAI2 are shown, fixing the tilt angle = 0.0, B = 5.0 nT, Np = 5/cc, and Vsw = 450 km/s.

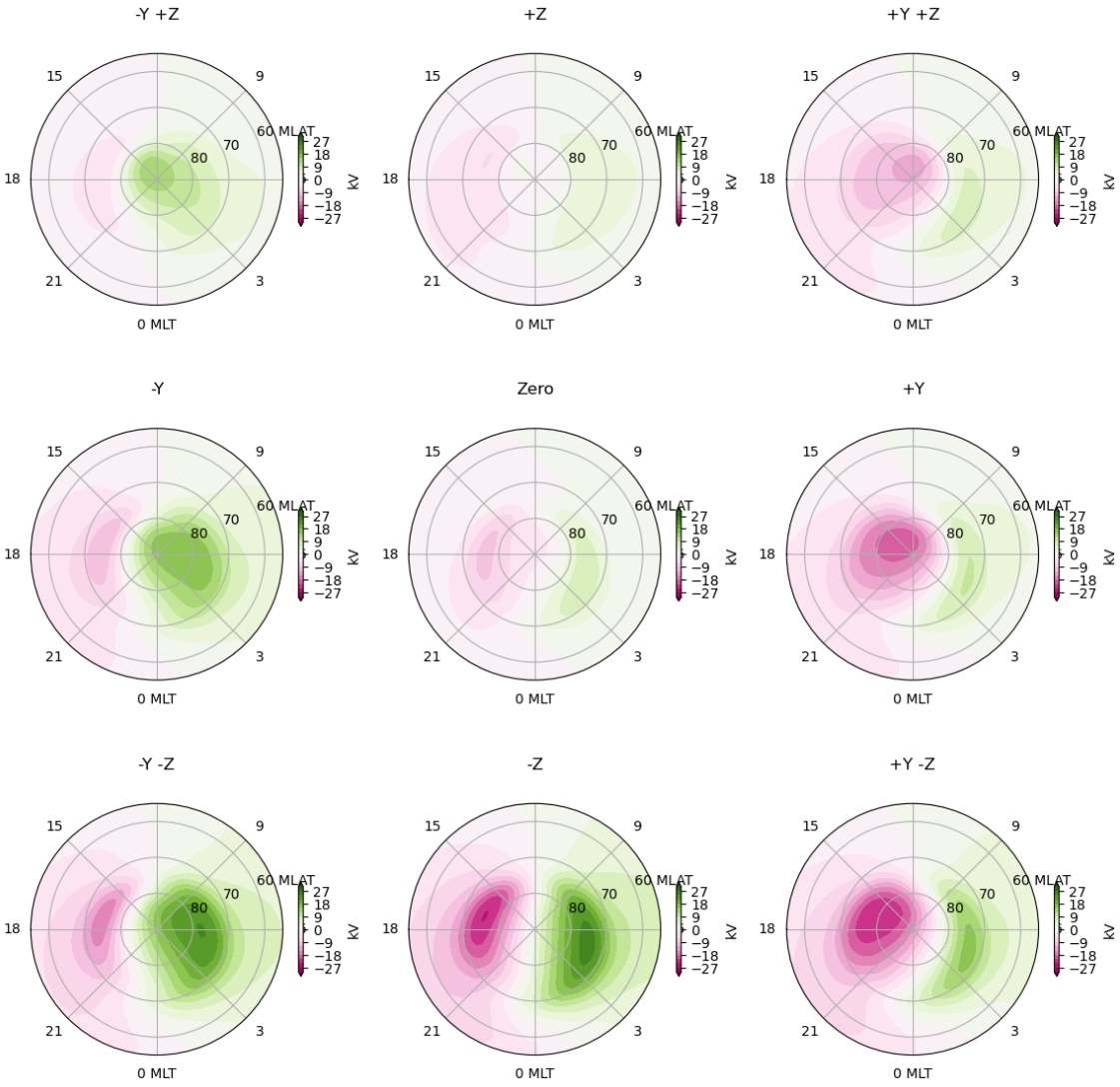

Figure 4. The IMF clock angle dependence of ionospheric potential in the northern hemisphere. Steady-state conditions from the SMRAI2 are shown, fixing the tilt angle = 0.0, B = 5.0 nT, Np = 5/cc, and Vsw = 450 km/s.

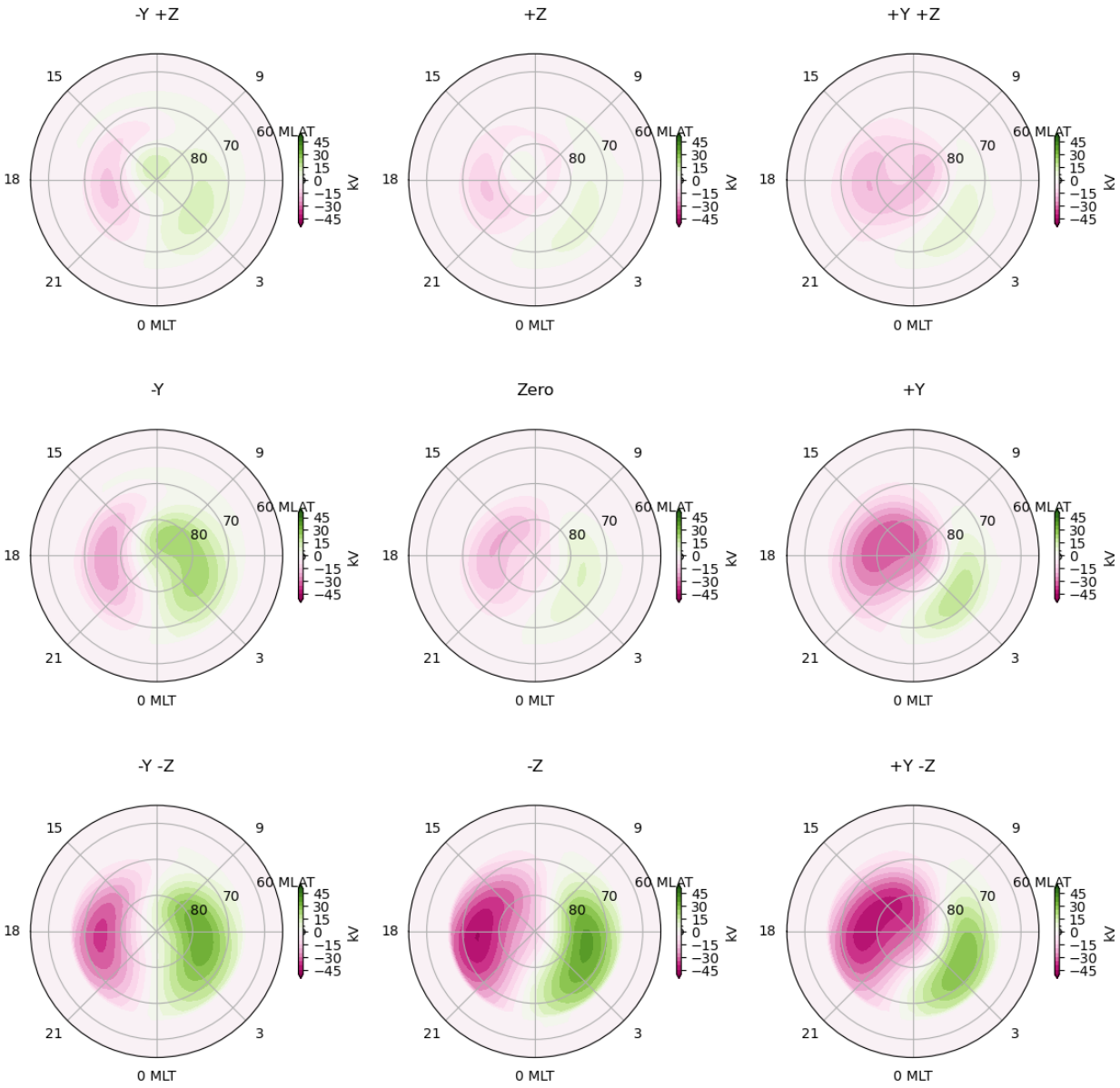

Figure 5. The IMF clock angle dependence of ionospheric potential in the northern hemisphere as obtained from the Weimer2K empirical model, with the tilt angle = 0.0, B = 5.0 nT, Np = 5/cc, and Vsw = 450 km/s.

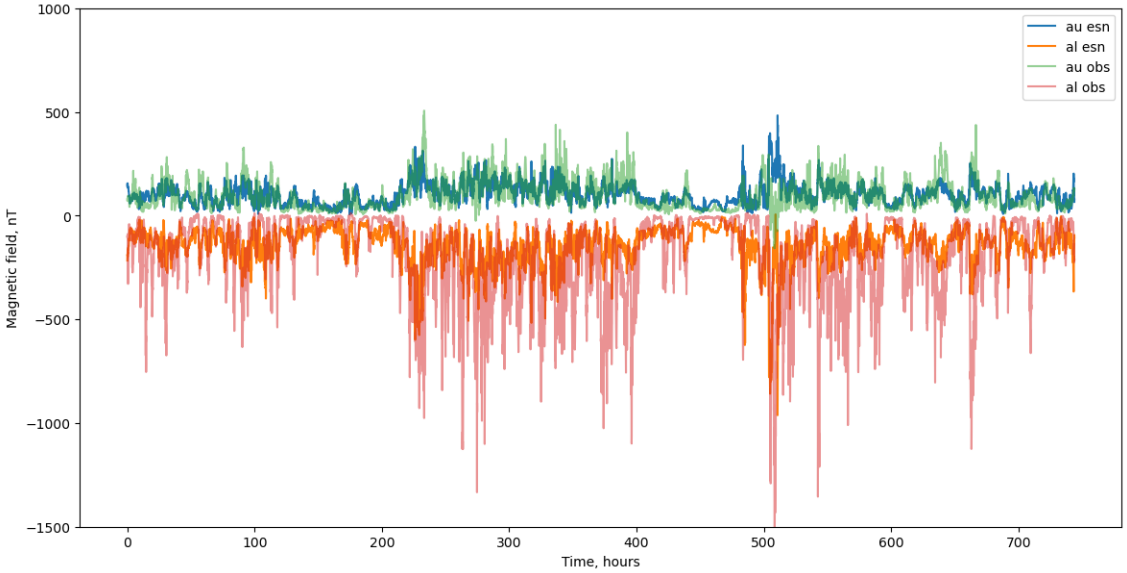

425

426 **Figure 6**. Example of the calculation of AU/AL indices by SMRAI2, compared with the
427 observed values, for the one-month time interval from October 1, 1999.
428

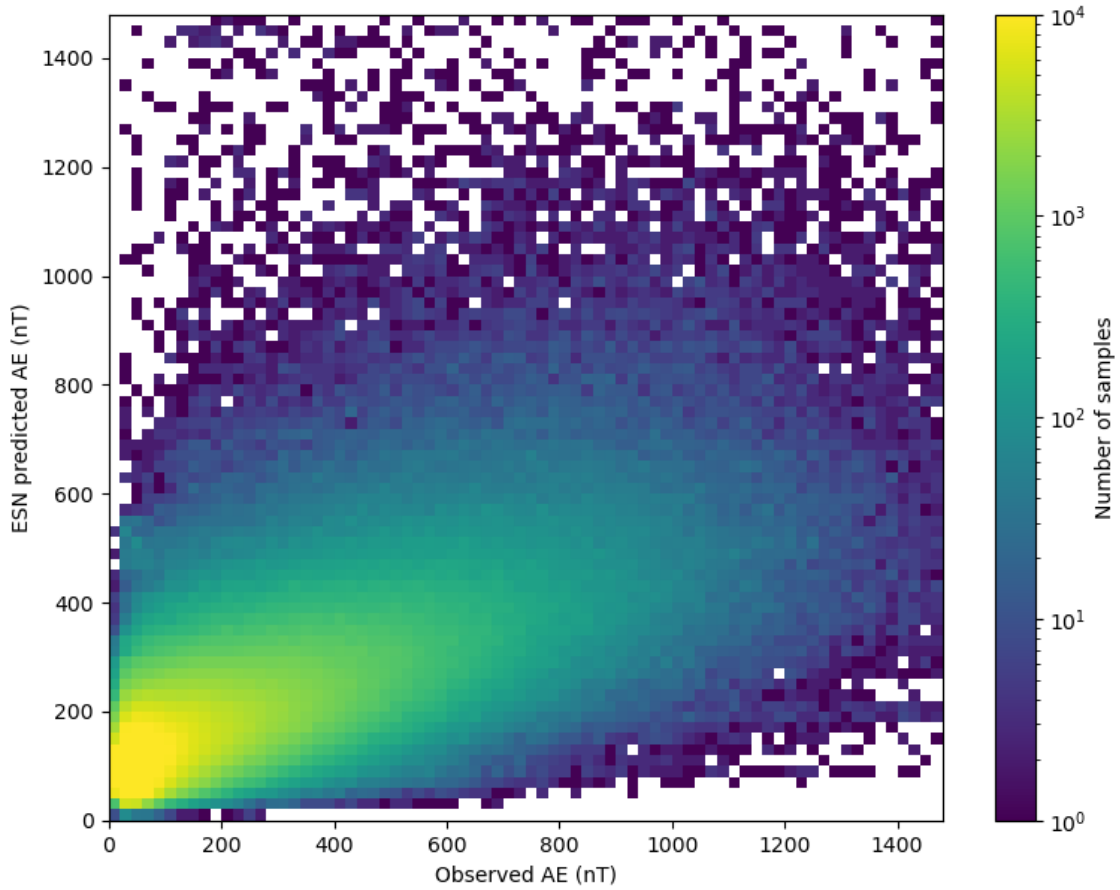

Figure 7. 2D histogram for the AE index as predicted by SMRAI2 against the observed AE index for the 15-year time interval from January 1, 2000.

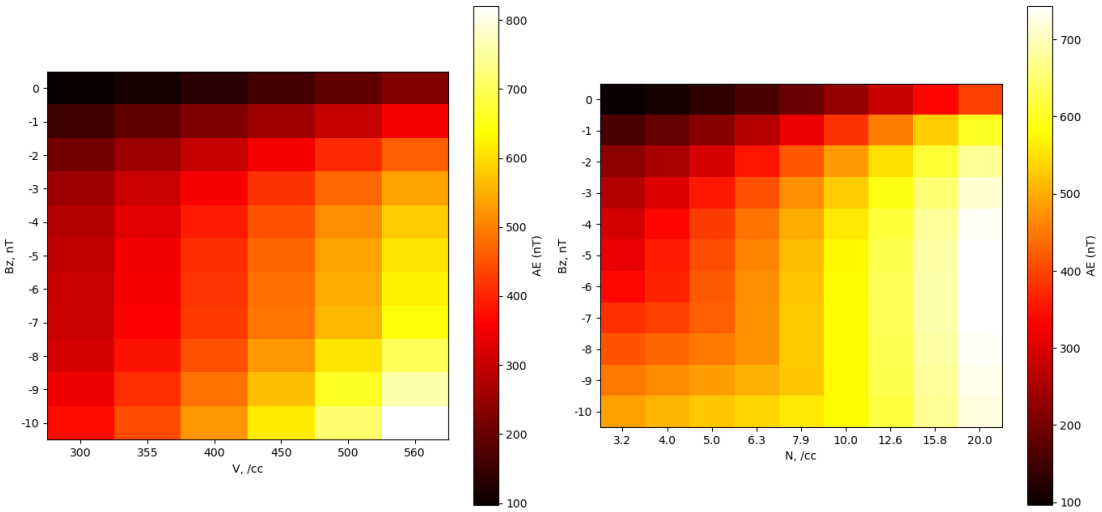

Figure 8. Heat map analysis of the SMRAI2-predicted AE peak intensity in the (left) IMF Bz-V space and in (right) IMF Bz-Np space.

435 **Table 1.** List of the selected events for training and testing the ESN model.
436

Start	End	# of days	Notes
2021/05/10	2021/05/15	5	Shock, moderate storm
2021/05/31	2021/06/03	4	Shock
2021/07/26	2021/07/29	4	northward IMF
2021/09/09	2021/09/12	4	northward IMF
2021/10/11	2021/10/14	4	Shock
2021/11/01	2021/11/06	6	Shock, intense storm
2021/11/25	2021/11/29	5	Shock
2022/01/30	2022/02/03	5	Shock
2022/03/11	2022/03/15	5	Shock
2022/03/28	2022/04/1	5	Shock
2022/08/15	2022/08/19	5	Shock
2021/12/01	2022/01/24	55	Long run for training
2022/06/10	2022/07/31	52	Long run for testing

437

438 **Table 2.** Specifications of SMRAI emulators version 1.0 (Kataoka et al., 2023) and version 2.0
439 (this study).
440

Parameters	SMRAI1	SMRAI2
Time resolution	10 min	5 min
Latitude resolution	~2 deg	~1 deg
Longitude resolution	11.25 deg	4.5 deg
Input solar wind parameters	By, Bz, Np, Vsw	Tilt, By, Bz, Np, Vsw
Training dataset	~10 days worth	~100 days worth
Hemisphere	North only	North and south

441